

Tracking nanoscale electric and magnetic singularities through three-dimensional space

NIR ROTENBERG,¹ BORIS LE FEBER,¹ TACO D. VISSER,^{2,3} AND L. KUIPERS^{1,*}

¹Center for Nanophotonics, FOM Institute AMOLF, Science Park 104, 1098 XG Amsterdam, The Netherlands

²Department of Electrical Engineering, Delft University of Technology, 2628 CD Delft, The Netherlands

³Department of Physics and Astronomy, VU University, 1081 HV Amsterdam, The Netherlands

*Corresponding author: kuipers@amolf.nl

Received 23 March 2015; revised 6 May 2015; accepted 7 May 2015 (Doc. ID 236707); published 4 June 2015

The study of light fields near nanophotonic structures continually reveals new fundamental features of light-matter interactions on the nanoscale, driving advances in fields ranging from nonlinear and quantum optics to biosensing. Here, we have succeeded in separately mapping the electric and magnetic fields. This allows us to present the first fully three-dimensional maps of the in-plane electromagnetic near fields of a photonic crystal waveguide, in experiment and theory. In these fields, we identify and study the spatial evolution of infinitesimally small optical entities: optical singularities. We discuss the topological properties of the local light fields in the vicinity of the singularities and show that the trajectory traced by each singularity through three-dimensional space is distinct. These results are an important step toward understanding the behavior of light at the nanoscale, opening up new avenues for on-chip control and detection of nanoscopic or quantum objects with structured light fields. © 2015 Optical Society of America

OCIS codes: (260.2110) Electromagnetic optics; (260.6042) Singular optics; (180.4243) Near-field microscopy.

<http://dx.doi.org/10.1364/OPTICA.2.000540>

1. INTRODUCTION

The study of light is unique in that although Maxwell's equations, which were formulated in the 1860s, completely describe the way in which light interacts with matter, we still discover new aspects of this interaction on a regular basis. Recently, more than a century and a half later, new solutions of these equations—for example, of knotted light fields [1–3] or Airy beams [4,5]—were found. Not only do these structured beams have fascinating and oftentimes surprising properties, but they are also technologically useful. Airy beams, for example, are nondiffracting, accelerating, and self-healing, and can be used as robust optical tweezers to trap and control particles [6]. Likewise, structured light can carry spin or orbital angular momentum (OAM) [7,8], and since this momentum can be transferred to, or from, particles [9], such beams are of great interest for quantum optical [10] and biophysical detection applications [11].

The emergence of nanophotonics has opened up a new arena for the study of light: the nanoscale. At these dimensions light-matter interactions are governed by geometry, and not only bulk material properties, lifting many of the limitations of far-field optics. The modulus of the in-plane wave vector of near fields, for example, is no longer limited, and as a consequence near fields are both highly localized to their sources and also can contain structure on length scales much shorter than the diffraction limit. In fact, unlike in the far field, the spatial evolution of the structure of the electric and magnetic near fields is often different [12]. Hence, when optical phenomena such as structured beams or

singularities [13] are studied in the near field [14–17], new and oftentimes surprising aspects of the behavior of light can be uncovered.

At the same time, there are clear practical advantages to bringing structured light fields to the nanoscale [18], particularly with solid-state structures that can be fabricated with high precision and reproducibility. The high degree of control over nanoscale geometry that is now possible allows for control over the structure of light fields on the same length scales as the objects with which they interact, for example, for biological or quantum technologies, and hence opens up new routes toward scalable platforms for these systems. Recently, in the context of quantum optics, researchers have begun exploring how nanophotonic structures whose near fields have circularly polarized regions can be used to interface, and even entangle, dipolar emitter states with photon pathways [19–23]. In fact, such light fields with a high degree of local chirality can also form the basis for ultrasensitive biosensors [24,25]. The success of these and other such applications is crucially dependent on our understanding of structured light fields at the nanoscale, a structure that is hard to observe, much less to study in detail.

In this work, we report on the three-dimensional spatial evolution of the wealth of nanoscopic features that may be found in the electromagnetic near fields of a photonic crystal waveguide (PhCW). To do so, we build on earlier work [12] and, for the first time, separate the electric and magnetic components in near-field optical measurements. This allows us to present the first

fully three-dimensional near-field measurements of not only the in-plane complex electric fields but also the in-plane magnetic fields above the PhCW. In these fields, we identify both phase and polarization singularities, whose properties and topological charges we can quantify. These measurements, which are in excellent agreement with rigorous electromagnetic simulations, reveal that each singularity follows a distinct trajectory through space. Our results both shed light on the complex evolution of highly structured light fields near nanophotonic structures and are important if these fields are to be used to control nanoscopic objects.

2. THREE-DIMENSIONAL NEAR-FIELD MAPPING

A PhCW is an ideal structure for our investigation. First, this type of waveguide is now routinely used to control the flow of light [26] and can be fabricated with extremely high quality and precision. Further, although there are no analytic solutions for the near-field distributions of these crystals, they can be numerically calculated [27]. These field distributions have a detailed structure on a subwavelength length scale and are known to contain electric polarization singularities at the surface of the PhCW [17].

Moreover, the evolution of the near fields of a PhCW through three-dimensional space can be extremely complex. This complexity arises as the PhCW mode is comprised of many Bloch

harmonics, each decaying with height at a different rate [28]; the larger the wave vector of a harmonic, the faster it decays. As a result, whereas the light field is highly structured close to the waveguide, far away from the surface we are left with a weak and relatively featureless light field. Such a metamorphosis of the field distributions cannot be found in far fields, and consequently it is reasonable to wonder whether the fine structure of these near fields might also evolve in a unique manner.

An investigation of the fine structure of the PhCW light fields presents several unique challenges. First, because we wish to study the spatial evolution of nanoscopic optical features, we need to map the near field with nanometer resolution in all three dimensions. Moreover, since we want to learn how the electromagnetic near field evolves, we need to simultaneously map both the electric and magnetic near fields. Crucially, this involves separating the electric and magnetic near-field signal from the measurements, where they are often tangled together. And, while a way of determining the sensitivity of a near-field probe to the electric and magnetic near fields exists [12], a successful unraveling of these two components from a near-field measurement has yet to be demonstrated. Finally, since we are interested in features in complex light fields, our measurements must resolve the phase, as well as the amplitude, of the near fields.

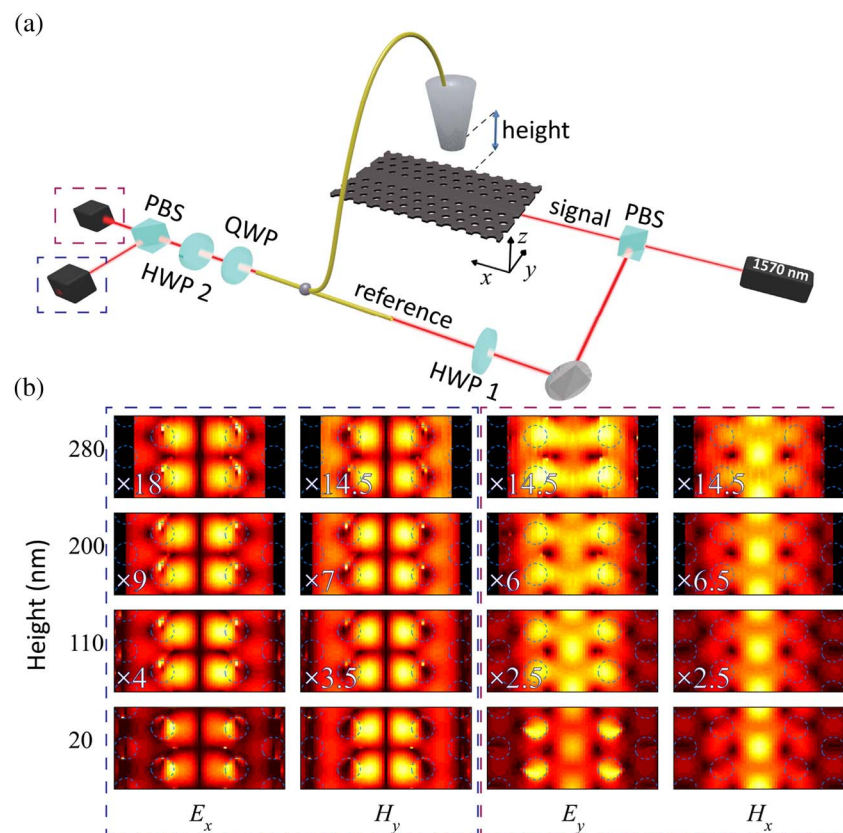


Fig. 1. Three-dimensional near-field microscopy. (a) Schematic of the near-field scanning optical microscope used to create three dimensional near-field maps above a PhCW. A polarizing beam splitter (PBS) splits the light into the signal branch, which is coupled into the PhCW, and a reference branch. The aperture probe tip scatters some of the near field into the fiber, where it is combined with the light in the reference branch and then detected on two photodiodes. A set of half-wave plates (HWPs) and a quarter-wave plate (QWP) ensure that the detector and sample frames are identical. (b) Measured field amplitudes of the in-plane electromagnetic near fields over 2 unit cells of the PhCW, at heights ranging from 20 to 280 nm above the waveguide surface. The scaling of each measurement, relative to the 20 nm plane, is indicated by the multiplication factor in the bottom left corner of each frame.

We create three-dimensional maps of the complex in-plane electromagnetic near fields of the PhCW, with nanoscopic resolution, using our home-built near-field scanning optical microscope [29], which we show in Fig. 1(a). We couple 1570 nm light into a PhCW (with a period $a = 420$ nm) and then place an aperture tip in its near field, thereby converting a small fraction of this near field into far-field radiation. By interfering this signal with a stable reference beam, we can retrieve the phase, as well as the amplitude, of the near field. We resolve the orientation of the near field using the standard polarization optics, shown in Fig. 1(a), which allow us to align the sample and measurement frames. Finally, to create three-dimensional maps of the near fields, we raster scan the tip of our aperture probe at heights ranging from 20 to 400 nm above the PhCW. The aperture probe that we use—essentially a tapered optical fiber that is coated with a thick, shielding layer of aluminum—is sensitive to both the electric (\mathbf{E}_{\parallel}) and magnetic (\mathbf{H}_{\parallel}) in-plane near fields. By comparing our measurements to rigorous numerical electromagnetic simulations [27], we are able to determine the efficiency with which the probe detects \mathbf{E}_{\parallel} and \mathbf{H}_{\parallel} [12]. Together, the experiments and calculations allow us to separate the electric and magnetic contributions from our measurements and map out the four in-plane field components at each height (using the procedure that we outline in Supplement 1).

In Fig. 1(b) we present the first fully three-dimensional map of the different in-plane components of the light field above a PhCW. In this figure we show the amplitude distributions of E_x , E_y , H_x and H_y , taken with nanoscopic step sizes below 100 nm in all three dimensions. From these images, we observe the similarities, but also the differences, between the various in-plane field components. Near the surface of the PhCW, for example, E_x and H_y are almost identical (except for the measurement artifacts near the holes), as are E_y and H_x . Farther away from the surface, however, we are able to image the subtle differences that emerge in the field distributions; 280 nm above the surface, for example, we see more field amplitude away from the center of the waveguide for H_y than for E_x . Likewise, at this height, the distribution of E_y has spread out farther than that of H_x . These observations agree with previously reported calculations for such waveguides [12].

3. OPTICAL SINGULARITIES IN NEAR FIELDS

A. Phase Singularities

The amplitude maps of the near fields only tell half of the story, with the rest being told by the phase maps. In Fig. 2 we show an example of both the calculated and measured complex in-plane fields 110 nm above the surface of the PhCW. In each frame we show 1.75 unit cells of either the amplitude $A(\mathbf{r})$ or the phase $\varphi(\mathbf{r})$ of the in-plane field components, with the left half ($y < 0$) taken from fully vectorial three-dimensional calculations (with no fitting parameters) [27] and the right half ($y > 0$) obtained from the measurements. As expected, due to the symmetry of the PhCW, the amplitudes of all components are mirror symmetric about the center of the waveguide ($y = 0$), while the phases of E_x and H_y show an odd symmetry, and those of E_y and H_x show an even symmetry, about this axis. The excellent agreement between the measurements and the calculations nicely demonstrates that it is possible to individually resolve the electric and magnetic near fields.

Within each unit cell, for every field component at this height, we find two pairs of phase singularities, which are points of undefined phase where the field amplitude is 0 [18]. Additionally, we find a line of undefined phase that necessarily occurs at $y = 0$ for the odd-symmetry components (E_x and H_y), whose amplitude there is also 0. We label the phase singularities, which can be found in the phase distributions shown in Figs. 2(e)–2(h) at locations where contours of constant phase intersect, as $p_1^{l,r}$ and $p_2^{l,r}$ [e.g., in Figs. 2(a) and 2(e)], and also show them in the amplitude maps. Each singularity carries a topological charge

$$s = \frac{1}{2\pi} \oint_C d\varphi, \quad (1)$$

where the closed circuit C is traversed in a counterclockwise manner, and φ denotes the phase of the field component. This charge denotes the number of units of OAM that are carried by the surrounding light fields. From the phase maps we calculate that for all singularities $s = \pm 1$ (see Table 1), and hence the total charge of each unit cell is 0. That is, unlike the far fields, where an entire beam carries OAM, in the near field of a PhCW the OAM is a property associated with specific regions within each unit cell.

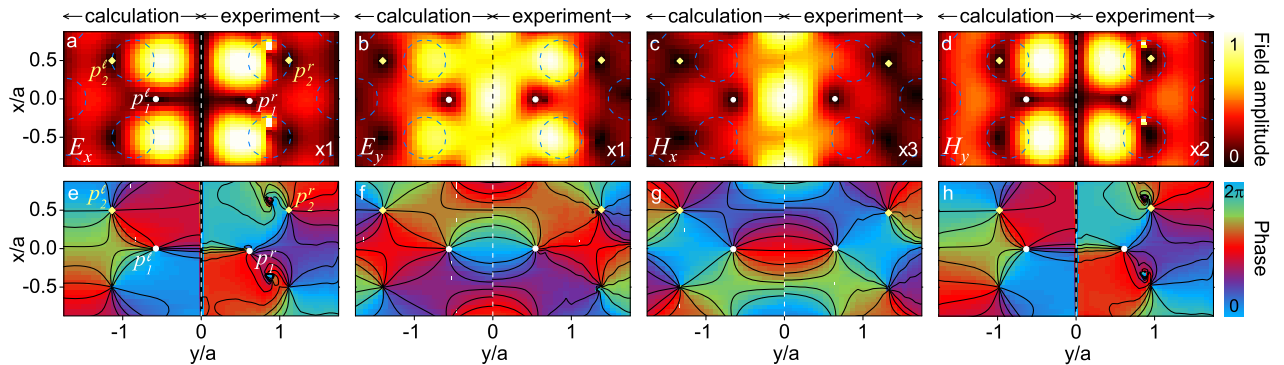


Fig. 2. Complex in-plane electromagnetic near fields above a PhCW: the calculated and measured amplitude (a)–(d) and corresponding phase (e)–(h) distributions of the in-plane electromagnetic field components 110 nm above the photonic crystal waveguide. The relative scaling of the amplitudes is shown the bottom right corner of (a)–(d) and the locations of the holes of the PhCW are indicated by the dashed blue curves. In (e)–(h), lines of constant phase are shown, and the phase singularities (denoted by solid symbols on all frames) occur where these lines intersect. In each frame we show the fields of two unit cells, marking the singularities in one of the unit cells. Calculations are shown on the left half of each frame, while the right half depicts the measurements.

Table 1. OAM Charge of the Phase Singularities in the In-Plane Fields^a

	E_x	E_y	H_x	H_y
p_1^ℓ	+1	-1	-1	+1
p_1^r	-1	+1	+1	-1
p_2^ℓ	-1	+1	+1	-1
p_2^r	+1	-1	-1	+1

^aNote that the edge dislocations at the center of E_x and H_y have an undefined s , since there is no way to close a loop about them.

Only objects with a characteristic length scale much shorter than the period of the PhCW (a) would, for example, begin to rotate when placed in the vicinity of the singularity; larger objects will experience the net effect of all the singularities, which is to say, nothing. This is in stark contrast to optical far fields, where OAM can be transferred from the light fields to larger objects, and in regions well away from any singularity.

It is also interesting to note that the singularities are located at different positions for the different field components. While in all cases p_1 and p_2 are separated by half a period in x , and indeed do not move in x as a function of height, they are found at differing y values. For example, p_1^ℓ of E_y is found at $x = 0$ and $y = (-0.56 \pm 0.07)a$, while for H_x it is at $x = 0$ and $y = (-0.66 \pm 0.07)a$. Here, the error is determined by the resolution of our measurements.

Having found phase singularities at one height, we now examine how these features evolve as a function of distance from the PhCW. Hence, we follow the trajectories of the singularities, through three-dimensional space, by repeating our measurements at heights ranging from 20 to 400 nm above the PhCW. In Fig. 3 we map these trajectories for all four phase singularities of the different in-plane fields, showing both experimental (symbols) and theoretical (curves) results. Because the symmetry of the PhCW about $y = 0$ ensures that each singularity pair is also mirrored (e.g., p_1^ℓ and p_1^r are equidistant from the center of the waveguide), we only show the position of one singularity from each pair, for each component. For our waveguide, we find that the position of these phase singularities can vary from $y = \pm 190$ nm to $y = \pm 890$ nm over the 400 nm of height that we investigate. Interestingly, the trajectory that a phase singularity follows is distinct, and there is a nontrivial relationship between how the electric field singularities and those associated with the magnetic fields evolve. This is in contrast to far fields, where there is typically a clearer relationship between \mathbf{E} and \mathbf{H} . In the near field of the photonic crystal, we can identify heights at which different phase singularities can be found at the same point (e.g., p_1^ℓ of E_x and E_y at a height of 100 nm, or of H_x and H_y at a height of 150 nm). At other heights the separation between the singularities can exceed the size of a typical quantum structure (tens of nanometers), or even that of a small classical object (hundreds of nanometers), like our near-field probe.

B. Polarization Singularities

In the rich structure of the PhCW light fields, phase is not the only quantity that can be singular. As shown by Burresi *et al.* for the electric field [17], we can also find polarization singularities in these near fields. Here, however, we are no longer limited to maps of the electric field, and we can also search for polarization singularities in the magnetic near fields. Unlike phase singularities,

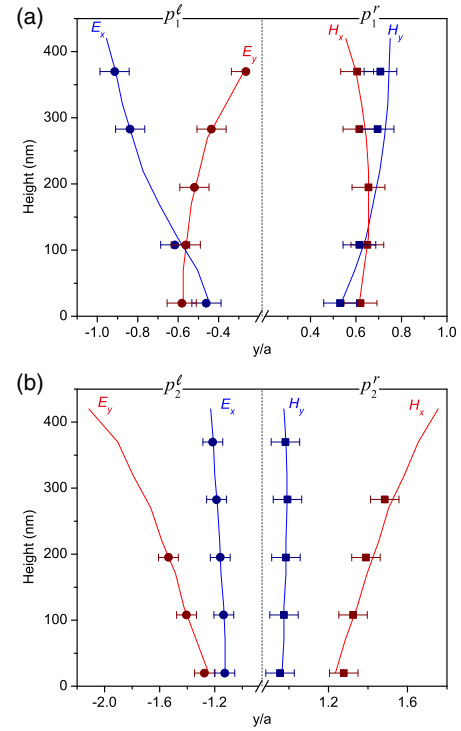


Fig. 3. Trajectories of phase singularities above the PhCW: the y position of the p_1 (a) and the p_2 (b) phase singularities for all in-plane field components as a function of height. In both panels the trajectories of the singularities determined from theoretical modeling are given by the solid curves, while the corresponding experimentally measured positions are shown by the symbols. The error bars represent the resolution of our measurements, and the period of the PhCW is $a = 420$ nm.

which can be found in individual vector components of the electric and magnetic fields, polarization singularities are properties of the total in-plane electric, or magnetic, field. As shown in Fig. 4, the end point of the field vector, at any point in space, traces out an ellipse over time. This ellipse can be characterized by its ellipticity,

$$\varepsilon(\mathbf{r}) = \tan\{\sin^{-1}[\sin(2\psi(\mathbf{r})) \sin(\delta(\mathbf{r}))]/2\}, \quad (2)$$

which denotes the ratio of the short to the long axis, and which ranges from +1 (right-circular polarization) to -1 (left-circular polarization) and represents linear polarization when $\varepsilon = 0$; and by its orientation angle,

$$\alpha(\mathbf{r}) = \{\tan^{-1}[\tan(2\psi(\mathbf{r})) \cos(\delta(\mathbf{r}))]/2\}, \quad (3)$$

which ranges from $+\pi/2$ to $-\pi/2$. In these equations $\psi(\mathbf{r}) = \tan^{-1}[A_x(\mathbf{r})/A_y(\mathbf{r})]$ and $\delta = \varphi_x(\mathbf{r}) - \varphi_y(\mathbf{r})$, and $A(\mathbf{r})$ and $\varphi(\mathbf{r})$ are the amplitude and phase, respectively, of either \mathbf{E} or \mathbf{H} .

In Fig. 4 we present the amplitude, α , and ε of the in-plane electric and magnetic fields, measured 110 nm above the surface of the PhCW, in which we look for polarization singularities. Polarization singularities are points where either the handedness (sign of ε) or orientation (α) of the polarization is undefined. The former occur where the polarization is linear ($\varepsilon = 0$) and are therefore known as L -lines, while the latter are of particular interest, as the light fields about points where the orientation of the polarization ellipse is undefined carry spin angular momentum. In analogy to phase singularities, these polarization singularities are

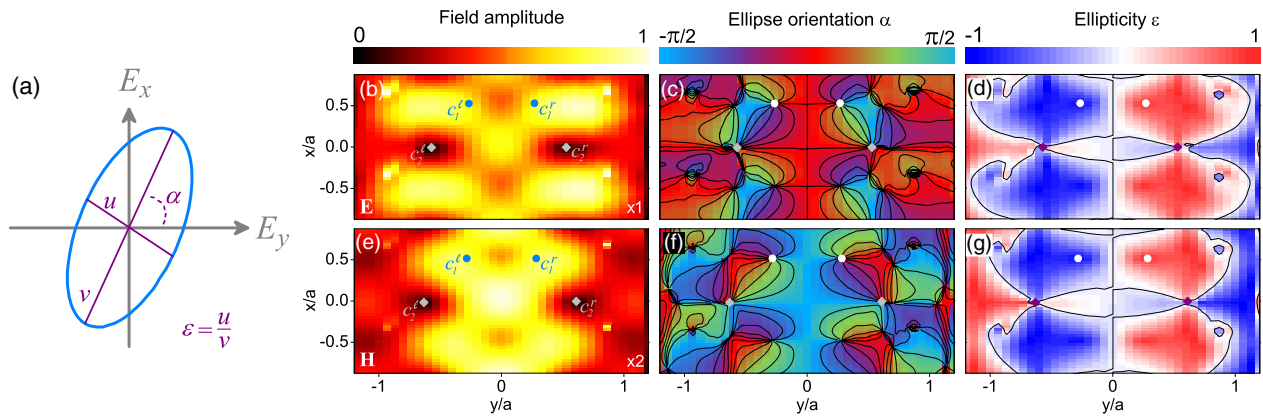


Fig. 4. Polarization state of the light 110 nm above the PhCW. (a) The polarization ellipse for the in-plane electric field, showing the ellipticity, ε , and the angle of orientation α ; (b)–(g), the amplitude, angle of orientation, and ellipticity of the in-plane electric fields (b)–(d) and in-plane magnetic fields (e)–(g). The scaling factors of the field amplitudes are shown in the bottom right corner of (b) and (e). The polarization singularities (C-points), $c_1^{\ell,r}$ and $c_2^{\ell,r}$, are marked by symbols in (b)–(g). Lines of constant α , which intersect at the singularities, are shown in (c) and (f), as are lines of linear polarization (L-lines) in (d) and (g).

found where lines of constant α intersect [Figs. 4(c) and 4(f)] and where the polarization is circular [$\varepsilon = \pm 1$ in Figs. 4(d) and 4(g)]. Consequently, these singular points are known as C-points, and, again, we find four per unit cell, which we denote $c_1^{\ell,r}$ and $c_2^{\ell,r}$. As we see from the ε maps in Figs. 4(d) and 4(g), each pair of C-points consists of singularities of opposite handedness, as is required for C-points that are separated by an L-line [see Fig. 4(d) as an example]. For example, for the electric field, the polarization at c_1^{ℓ} is left-handed, while at c_1^r it is right-handed. We note that only at c_1 of the electric field does the associated out-of-plane component vanish (i.e., $E_z \rightarrow 0$), and hence only this point is a true polarization singularity in three-dimensional space (see Supplement 1). Interestingly, and unlike the case of the phase singularities, here we find points c_1 in regions of high in-plane field amplitude. In analogy with the phase singularities, about which a nanoscopic object would rotate, an object placed at a C-point would begin to spin (in place). Likewise, it is important

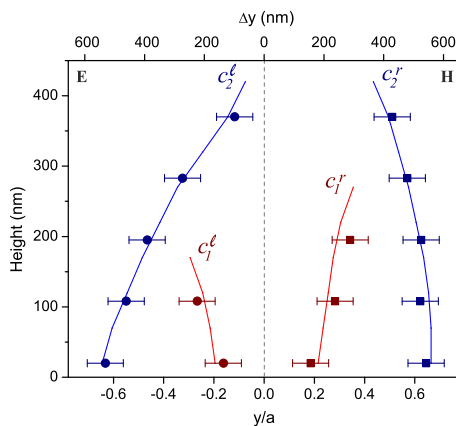


Fig. 5. Trajectories of the polarization singularities. The left side shows two of the singularities associated with the in-plane electric field, and the right side shows two associated with the in-plane magnetic field. Both calculations (curves) and measurements (symbols) are shown, and the error bars on the latter are due to the experimental resolution. The bottom axis denotes the position of each singularity, while in the top we show the separation between each singularity pair.

to know if the object is electric or magnetic in nature, since the C-points associated with the electric and magnetic fields are typically found in different locations.

It is also important to know the height above the waveguide at which an object would interact with the PhCW light field, and not just whether the object is electric or magnetic in nature. To illustrate this, we show the trajectories that the C-points follow through space in Fig. 5, where again we see that each trajectory is unique. As is evident in this figure, while these polarization singularities appear as points in a given plane, in three-dimensional space they trace out lines (while L-lines trace out surfaces). Following these trajectories is particularly important for points c_1 , which are located in regions of high field, but which are also only found relatively close to the PhCW. For the electric field, we find these singularities up to a height of about 175 nm, while for the magnetic field they are present up to about 275 nm. The vanishing of these singularities, without annihilation [30], is intriguing, as no analogous behavior has either been observed or predicted in the far field. This vanishing may, initially, seem problematic, since each C-point carries a topological charge (see Supplement 1), which is a conserved property of the light field. As we noted above, at each height above the PhCW we find pairs of C-points, which are mirrored about the center of the waveguide at $y = 0$, and which carry opposite charge. Since both singularities in a pair vanish simultaneously, the charge of the light field is conserved, remaining 0 at all heights. In fact, this spontaneous and simultaneous disappearance of separate singularities has been theoretically predicted [31] but never before observed.

Furthermore, we observe that the trajectories of c_1^{ℓ} and c_1^r diverge for both \mathbf{E} and \mathbf{H} , suggesting that for future applications that require fields with a nonzero topological charge, it might be desirable to work at greater heights. For example, the separation between c_1^{ℓ} and c_1^r , which we denote Δy , is only 160 nm at a height of 20 nm above the PhCW, but it grows to 250 nm at a height of 170 nm. We recall, however, that the fields are evanescent, and hence their amplitude decreases at greater heights, alluding to a balance between C-point separation and field strength that must be taken into account in any potential application (see Supplement 1).

4. CONCLUSION

In summary, we presented the first fully three-dimensional measurements of the complex vector electromagnetic near field of a PhCW, having developed a procedure to separate and map the electric and magnetic near fields simultaneously. In these measurements we identify two types of optical singularities, and we directly observe the trajectories that these singularities follow through space. There are many nanophotonic structures other than PhCWs whose near fields can contain optical singularities, as is nicely demonstrated by recent investigations into optical singularities in plasmonic near fields [31,32]. Our technique can be readily applied to these systems, for the study both of optical singularities and of the evolution of the light fields themselves.

Our results are in excellent agreement with calculations, and they highlight the nontrivial relation between the electric and magnetic near fields of nanophotonic structures. That is, using nanoscopic geometry, it is possible to create a subwavelength fine structure in light fields that behaves in a manner that cannot always be reproduced in the far field. Although we have focused on near fields, optical singularities are a ubiquitous phenomenon that can be found at all scales, from the nanoscale in a controllable manner in our photonic crystals to everyday dimensions [33], and recently even to astronomical scales [34].

To conclude, not only do our results improve our understanding of the behavior of light near nanophotonic structures, but they are expected to be important for emerging technologies. The light fields that we observe and study can in fact be thought of as possessing a local chirality, although the underlying two-dimensional waveguide is achiral. This phenomenon has been recently predicted [35] and observed [36] in plasmonic structures. Our system, in contrast to the earlier works, is completely dielectric, and while it does not display the large field enhancement inherent in plasmonic systems, it also does not suffer from high losses.

Also, from a technological viewpoint, fields with large local chirality are very desirable. Such fields can be used to selectively detect different isomers, and hence can form the basis of ultrasensitive biosensors [24,25]. Moreover, recent studies of the interaction of dipoles with the structured light fields near nanophotonic waveguides have revealed directional emission when the dipoles are placed in regions where the light fields are circularly polarized [19,21], exactly as they are about C-points. Further, theoretical studies have predicted that such controlled, directional emission can be used to create scalable quantum architecture [22,23]. Our insights into the structure and evolution of nanoscale light fields will help unlock the full potential of nanophotonic structures for quantum information processing, or the manipulation of nanoscopic objects.

EU FET project “SPANGL4Q”; European Research Council (ERC) (240438-CONSTANS); Foundation for Fundamental Research on Matter (Foundation for Fundamental Research on Matter).

See Supplement 1 for supporting content.

REFERENCES

- J. Leach, M. R. Dennis, J. Courtial, and M. J. Padgett, “Laser beams: knotted threads of darkness,” *Nature* **432**, 165 (2004).
- W. T. M. Irvine and D. Bouwmeester, “Linked and knotted beams of light,” *Nat. Phys.* **4**, 716–720 (2008).
- H. Kedia, I. Bialynicki-Birula, D. Peralta-Salas, and W. T. Irvine, “Tying knots in light fields,” *Phys. Rev. Lett.* **111**, 150404 (2013).
- S. Jia, J. Lee, J. W. Fleischer, G. A. Siviloglou, and D. N. Christodoulides, “Diffusion-trapped Airy beams in photorefractive media,” *Phys. Rev. Lett.* **104**, 253904 (2010).
- I. Kaminer, R. Bekenstein, J. Nemirovsky, and M. Segev, “Nondiffracting accelerating wave packets of Maxwell’s equations,” *Phys. Rev. Lett.* **108**, 163901 (2012).
- D. G. Grier, “A revolution in optical manipulation,” *Nature* **424**, 810–816 (2003).
- A. T. O’Neil, I. MacVicar, L. Allen, and M. J. Padgett, “Intrinsic and extrinsic nature of the orbital angular momentum of a light beam,” *Phys. Rev. Lett.* **88**, 053601 (2002).
- M. V. Berry and M. R. Dennis, “Polarization singularities in isotropic random vector waves,” *Proc. R. Soc. A* **457**, 141–155 (2001).
- H. He, M. E. J. Friese, N. R. Heckenberg, and H. Rubinsztein-Dunlop, “Direct observation of transfer of angular momentum to absorptive particles from a laser beam with a phase singularity,” *Phys. Rev. Lett.* **75**, 826–829 (1995).
- X. Cai, J. Wang, M. J. Strain, B. Johnson-Morris, J. Zhu, M. Sorel, J. L. O’Brien, M. G. Thompson, and S. Yu, “Integrated compact optical vortex beam emitters,” *Science* **338**, 363–366 (2012).
- M. P. J. Lavery, F. C. Speirits, S. M. Barnett, and M. J. Padgett, “Detection of a spinning object using light’s orbital angular momentum,” *Science* **341**, 537–540 (2013).
- B. le Feber, N. Rotenberg, D. M. Beggs, and L. Kuipers, “Simultaneous measurement of nanoscale electric and magnetic optical fields,” *Nat. Photonics* **8**, 43–46 (2013).
- M. R. Dennis, K. O’Holleran, and M. J. Padgett, “Singular optics: optical vortices and polarization singularities,” *Prog. Opt.* **53**, 293–363 (2009).
- A. Minovich, A. E. Klein, N. Januts, T. Pertsch, D. N. Neshev, and Y. S. Kivshar, “Generation and near-field imaging of Airy surface plasmons,” *Phys. Rev. Lett.* **107**, 116802 (2011).
- A. Libster-Hershko, I. Epstein, and A. Arie, “Rapidly accelerating Mathieu and Weber surface plasmon beams,” *Phys. Rev. Lett.* **113**, 123902 (2014).
- M. L. M. Balistreri, J. P. Korterik, L. Kuipers, and N. F. van Hulst, “Local observations of phase singularities in optical fields in waveguide structures,” *Phys. Rev. Lett.* **85**, 294–297 (2000).
- M. Burreli, R. J. P. Engelen, A. Opheij, D. van Oosten, D. Mori, T. Baba, and L. Kuipers, “Observation of polarization singularities at the nanoscale,” *Phys. Rev. Lett.* **102**, 033902 (2009).
- D. L. Andrews, *Structured Light and Its Applications* (Academic, 2008).
- J. Petersen, J. Volz, and A. Rauschenbeutel, “Chiral nanophotonic waveguide interface based on spin-orbit interaction of light,” *Science* **346**, 67–71 (2014).
- R. Mitsch, C. Sayrin, B. Albrecht, P. Schneeweiss, and A. Rauschenbeutel, “Quantum state-controlled directional spontaneous emission of photons into a nanophotonic waveguide,” *Nat. Commun.* **5**, 5713 (2014).
- B. le Feber, N. Rotenberg, and L. Kuipers, “Nanophotonic control of circular dipole emission,” *Nat. Commun.* **6**, 6695 (2015).
- A. B. Young, A. Thijssen, D. M. Beggs, L. Kuipers, J. G. Rarity, and R. Oulton, “Polarization engineering in photonic crystal waveguides for spin-photon entanglers,” arXiv: 1406.0714 (2014).
- I. Söllner, S. Mahmoodian, S. L. Hansen, L. Midolo, A. Javadi, G. Kiršanskė, T. Pregnolato, H. El-Ella, E. H. Lee, J. D. Song, S. Stobbe, and P. Lodahl, “Deterministic photon-emitter coupling in chiral photonic circuits,” arXiv: 1406.4295 (2015).
- E. Hendry, T. Carpy, J. Johnston, M. Popland, R. V. Mikhaylovskiy, A. J. Laphorn, S. M. Kelly, L. D. Barron, N. Gadegaard, and M. Kadodwala, “Ultrasensitive detection and characterization of biomolecules using superchiral fields,” *Nat. Nanotechnol.* **5**, 783–787 (2010).
- Y. Tang and A. E. Cohen, “Enhanced enantioselectivity in excitation of chiral molecules by superchiral light,” *Science* **332**, 333–336 (2011).
- J. D. Joannopoulos, S. G. Johnson, J. N. Winn, and R. D. Meade, *Photonic Crystals: Molding the Flow of Light* (Princeton University, 2011).
- S. G. Johnson and J. D. Joannopoulos, “Block-iterative frequency-domain methods for Maxwell’s equations in a planewave basis,” *Opt. Express* **8**, 173–190 (2001).
- H. Gersen, T. J. Karle, R. J. P. Engelen, W. Bogaerts, J. P. Korterik, N. F. van Hulst, T. F. Krauss, and L. Kuipers, “Direct observation of Bloch

- harmonics and negative phase velocity in photonic crystal waveguides," *Phys. Rev. Lett.* **94**, 123901 (2005).
29. N. Rotenberg and L. Kuipers, "Mapping nanoscale light fields," *Nat. Photonics* **8**, 919–926 (2014), and references therein.
 30. R. W. Schoonover and T. D. Visser, "Polarization singularities of focused, radially polarized fields," *Opt. Express* **14**, 5733–5745 (2006).
 31. H. F. Schouten, T. D. Visser, G. Gbur, D. Lenstra, and H. Blok, "Connection between phase singularities and the radiation pattern of a slit in a metal plate," *Phys. Rev. Lett.* **93**, 173901 (2004).
 32. A. de Hoogh, N. Rotenberg, and L. Kuipers, "Optical singularities in plasmonic fields near single subwavelength holes," *J. Opt.* **16**, 114004 (2014).
 33. J. F. Nye, *Natural Focusing and Fine Structure of Light: Caustics and Wave Dislocations* (CRC Press, 1999).
 34. BICEP2 Collaboration, "Detection of B-mode polarization at degree angular scales by BICEP2," *Phys. Rev. Lett.* **112**, 241101 (2014).
 35. T. J. Davis and E. Hendry, "Superchiral electromagnetic fields created by surface plasmons in nonchiral metallic nanostructures," *Phys. Rev. B* **87**, 085405 (2013).
 36. S. Hashiyada, T. Narushima, and H. Okamoto, "Local optical activity in achiral two-dimensional gold nanostructures," *J. Phys. Chem. C* **118**, 22229–22233 (2014).